Philosophical Magazine Letters
Vol. 88, No. 8, August 2008, 553–565

Downloaded By: [Oak Ridge National Laboratory] At: 20:48 4 September 2009

Neutron and X-ray diffraction studies and cohesive interface model of the fatigue crack deformation behavior

Rozaliya Barabash[ab]*, Yanfei Gao[cd], Yinan Sun[c], Soo Yeol Lee[c], Hahn Choo[ac], Peter K. Liaw[c], Donald W. Brown[e] and Gene E. Ice[a]

[a]*Materials Science and Technology Division, Oak Ridge National Laboratory, Oak Ridge, TN, USA;* [b]*Center for Material Processing, The University of Tennessee, Knoxville, TN, USA;* [c]*Materials Science and Engineering Department, The University of Tennessee, Knoxville, TN, USA;* [d]*Computer Science and Mathematics Division, Oak Ridge National Laboratory, Oak Ridge, TN, USA;* [e]*Materials Science and Technology Division, Los Alamos National Laboratory, Los Alamos, NM, USA*

(*Received 15 May 2007; final version received 30 June 2008*)

The crack-tip deformation behavior during a single overload, fatigue test of ferritic stainless steel, and Ni-based HAYNES 230 superalloy is studied at different structural levels using (1) neutron-diffraction, from which both the elastic-lattice strain and volume-averaged total dislocation densities are obtained, (2) polychromatic X-ray microdiffraction to probe the geometrically necessary dislocations and boundaries distribution, and (3) an irreversible and hysteretic cohesive interface model which has been implemented into a finite element framework to simulate the stress/strain evolution near the fatigue crack tip. Neutron strain measurements and finite element simulations are in qualitative agreement on the macroscopic length scale. Large plastic deformation induced by the overload and the resulting compressive residual strains are observed in front of the crack tip after the overload, and are the principal reason for the fatigue-crack-growth retardation. Strong strain gradients surrounding the crack propagation result in the formation of a high density of geometrically necessary dislocations near the fractured surface and cause local lattice rotations on the submicron level.

Keywords: crack growth; dislocations; FEM; neutron diffraction; X-ray diffraction

1. Introduction

The ability to predict the growth rate of fatigue cracks is of critical importance for the development of damage-tolerant designs and residual-life assessments [1]. The commonly used constant-amplitude loading profile in fatigue tests is insufficient to address the complicated working conditions in service. For example, it has been shown that a single overload in fatigue-loading history can result in a period of crack-growth retardation, which can be understood in the context of the plasticity-induced crack-closure mechanism [2–11]. Measurements of the elastic and plastic strain distributions near the crack tip

*Corresponding author. Email: barabashr@ornl.gov

ISSN 0950–0839 print/ISSN 1362–3036 online
© 2008 Taylor & Francis
DOI: 10.1080/09500830802311080
http://www.informaworld.com

can provide an experimental basis for the development of predictive models of the fatigue crack propagation behavior. However, owing to the small plastic zone size, direct measurements are challenging. Thus, the understanding of the fatigue overload effects remains largely qualitative in nature.

This work aims to study the elastic/plastic strain and their gradients together with dislocation distributions around a fatigue crack by neutron diffraction (ND), polychromatic X-ray microdiffraction (PXM) and finite element (FE) simulations based on a cohesive interface model. Because of the deep penetration capability of neutron beams, ND allows bulk measurements with a typical spatial resolution in the order of millimeter. Substructure neutron diffraction analysis in polycrystalline materials has several advantages: (1) due to the large scattering volume, neutron diffraction gives the bulk averaged values of the dislocation substructure parameters; (2) it is applicable for coarse-grained samples (with the grains size $\geq$80 μm); (3) results are not influenced by surface effects; (4) as the atomic scattering power is almost independent of the scattering angle, it is possible to assess higher diffraction orders compared to X-ray diffraction. Volume-averaged elastic lattice strains in a polycrystalline material under residual or applied stresses can be determined from the shift of the diffraction peaks [12–19], and the total dislocation density can be estimated from a peak profile analysis of the diffraction profiles.

However, neutron diffraction measurements from polycrystalline materials are not sensitive to the presence of geometrically necessary dislocations (GNDs) and geometrically necessary boundaries (GNBs). To obtain an understanding about the GNDs and GNBs arrangement at the microscale, the polychromatic X-ray microbeam measurements with a submicron spatial resolution were performed. X-ray microdiffraction can map the three-dimensional (3D) spatially-resolved dislocation character within a submicron volume. It is specifically designed to get information about the GNDs, GNBs, and strain gradients, which is not currently possible with neutron diffraction [20–22]. The measured lattice strains and their evolution during overload can be compared to the finite element simulations that are based on an irreversible, hysteretic cohesive interface model [23–26]. This type of continuum model and the application of both neutron and X-ray diffraction techniques provide multiscale information about an overload influence on the plastic deformation mechanisms during crack propagation and crack closure phenomena.

2. Experimental details

The materials used in this study are ferritic 316 stainless steel and Ni-based HAYNES 230 superalloy with an average grain size of ~80 μm for both materials. Compact-tension (CT) specimens (width 50.8 mm and thickness 6.35 mm) were machined and fatigue tested with a frequency of 10 Hz (Figure 1a). The maximum and minimum loads are 6,667 N and 667 N, respectively. When the crack length reached 22.8 mm, an overload of 8,889 N was applied (Figure 1b). ND measurements were performed on various load points (LP) during tensile loading and unloading cycles using the Spectrometer for Materials Research at Temperature and Stress (SMARTS) at the Los Alamos Neutron Science Center (LANSCE) [27]. The CT specimens were aligned such that the tensile load axis was 45° from the incident beam and, thus, the diffraction vectors associated with the two detector banks were parallel to the in-plane (IP) (parallel to the loading direction) and through-thickness (TT) directions of the sample (Figure 1c). The incident neutron beam

Downloaded By: [Oak Ridge National Laboratory] At: 20:48 4 September 2009

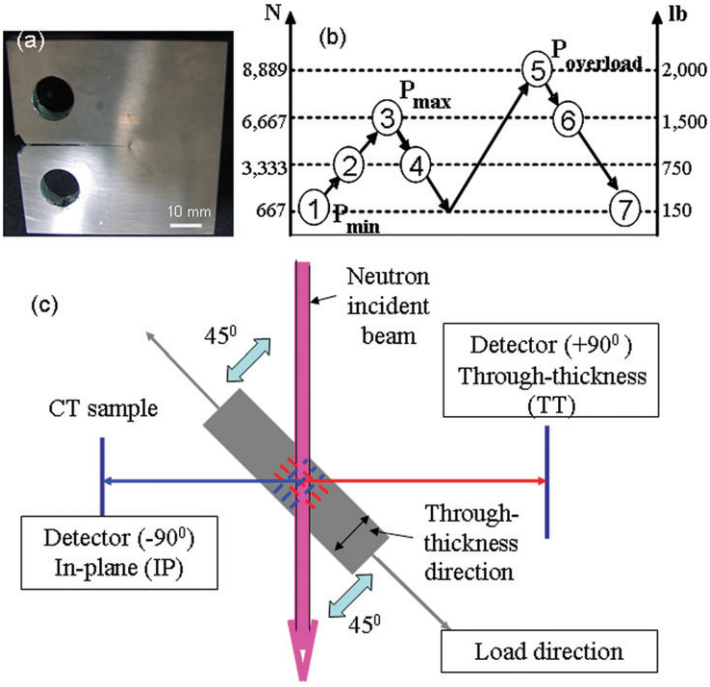

Figure 1. Optical image of the sample (a); different load points before and after overload (b); and the sketch of the neutron diffraction geometry (c).

was defined by 2 mm and 1 mm (along the crack length) slits, and the diffracted beams were collimated using 2 mm radial collimators, resulting in a 4 mm^3 gauge volume. Thirty-two diffraction patterns were recorded along the crack length, as shown in Figure 2. The interatomic spacing was determined by the Rietveld refinement [28] of the diffraction patterns. The lattice strains caused by the fatigue deformation and overloading, $\varepsilon = (a - a_0)/a_0$, were obtained along both IP and TT directions, where a is the lattice parameter, and a_0 is a 'stress-free' reference measured at the corner of the CT specimen. The severity of the plastic deformation at the macroscale was estimated from the ND measurements along both IP and TT directions by peak-profile analysis. Different peak profile analyses approaches are described in references [29–45].

Polychromatic X-ray microdiffraction (PXM) was used for a spatially-resolved investigation of the GNDs arrangement near the crack tip. PXM was performed with a focused ~0.5 μm diameter polychromatic synchrotron beam, which hit the sample surface at 45° incidence. The Laue diffraction patterns were recorded with a charge-coupled device (CCD) area detector placed at an angle of 90° relative to the incident beam [20–22]. Two-dimensional (2D) maps were recorded along the crack propagation path of the Ni-based superalloy with 1 μm step size in the directions parallel and perpendicular to the fractured surface of the crack. In special locations with a high density of geometrically necessary dislocations, 3D resolved measurements were performed with a special differential aperture microscopy technique (DAXM) [20–22]. These measurements determine the depth-dependent strain-gradient distributions near the crack.

Downloaded By: [Oak Ridge National Laboratory] At: 20:48 4 September 2009

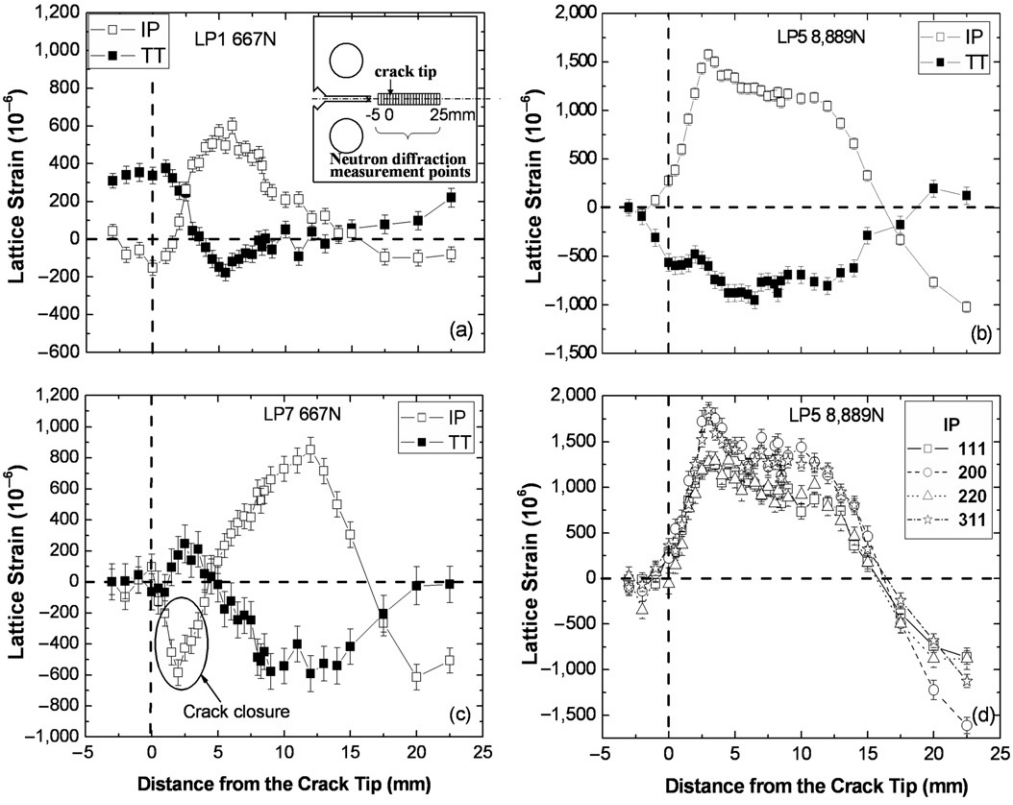

Figure 2. Elastic lattice strain distributions at the minimum loads before (a), during (b), and after the overload (c). In-plane lattice strain distributions in the different (*hkl*) directions during the overload (d). The inset in (a) shows the neutron measurement positions behind and in front of the crack tip.

3. Results and discussion

3.1. *Volume average parameters from neutron diffraction*

The lattice strain profiles before (LP1), at (LP5) and after (LP7) overload are shown in Figure 2(a–c), respectively. Before the overload (Figure 2a), small compressive strains (with a maximum of -200×10^{-6} or $\mu\varepsilon$) are observed within about 3 mm around the crack tip along the IP direction. At the overload (LP5), the large tensile strains (with a maximum of 1,600 $\mu\varepsilon$) are found ahead of the crack tip (Figure 2b). After the application of the overload (Figure 2c), the compressive lattice strains of up to -600×10^{-6} are observed within about 4 mm in front of the crack tip. Had it not been for the overload, the corresponding lattice strain curves in the next cycle would have shown little differences from those presented in Figure 2(a). Tensile strains are observed between 4 mm and 16 mm in front of the crack tip (Figure 2c), and the strains become compressive at about 16 mm because of the finite specimen size. Consequently, the large compressive strains in front of the crack tip strongly suggest that a crack-closure phenomenon is associated with the overload-induced large plastic deformation. The lattice strain profiles along the TT direction had an opposite sign from those along IP direction. Apparently, the strain

Downloaded By: [Oak Ridge National Laboratory] At: 20:48 4 September 2009

distributions in the IP and TT directions are related through the residual stress distribution, which is governed by the elastic–plastic properties of the material and the fatigue loading history.

The dislocation structure parameters were determined from peak profile analysis, which is a generally accepted method for the integrated characterization of the dislocation substructure [31–47]. In time-of-flight diffraction, the diffraction-line profile and the diffraction peak-widths include contributions from dislocations, stacking faults, small coherent regions in the sample, macroscopic strain gradients, and the distribution of intergranular strains in the region of the plastic deformation. In the first approximation, strain or size broadening can be described by Gaussian or Lorentzian functions, respectively [31–48]. The general method relating the neutron or X-ray diffracted intensity distribution to particular dislocation arrangements for different crystal symmetries was described in detail by Wilkens [34], Krivoglaz [35], Krivoglaz et al. [36], Barabash and Krivoglaz [37], Wilkens et al. [41], Groma and Szekely [42], Ungar et al. [43], Mughrabi [44], and Mughrabi et al. [45].

The most direct method to determine the dislocation density is based on the analyses of the shape of the tails of diffraction peaks [35–45]. However, the diffraction peak intensity at the tails of the peak is small (approximately equal to several percent of the maximal intensity). In the neutron diffraction measurements of the present study, the signal to noise ratio at the tails of the peak was small. Therefore, the detailed method developed by Groma and Szekely [42] and Ungar et al. [43] for the analysis of the tails of the intensity distribution could not be reliably applied. For this reason, a less direct method in which the dislocation induced broadening of the central part of the X-ray line was used in this study to characterize the dislocation substructure evolution. According to the references [35–38] the *central part* of the peak profile of the polycrystalline sample with randomly distributed and/or weakly correlated statistically stored (SS) dislocations can be described by a Gaussian function:

$$I(\mathbf{Q}) = I_{hkl}\ \mathrm{Exp}\left[-\frac{\pi q_{hkl}^2}{\sigma_{hkl}^2}\right], \quad \text{for } q_{hkl} < \sigma_{hkl} \tag{1}$$

$$\sigma_{hkl}^2 = 0.5n(Q\mathbf{b})^2\chi(hkl); \tag{2}$$

here σ_{hkl} is the full width at half maximum of the peak (FWHM) which depends on the total dislocation density, n, norm of the diffraction vector, Q, Burgers vector, $\mathbf{b}$, and on a contrast factor, $\chi(hkl)$. The contrast factor depends on the activated dislocation's slip systems, elastic moduli of the matrix and (hkl) of the peak.

However, a pure random dislocation arrangement is practically never observed. According to Mughrabi [44] and Mughrabi et al. [45], plastic deformation results in the formation of the so-called cell-wall structure with a high-dislocation density within the cell-walls and relatively low density in the cell interior. The existence of the cell-wall structure in the dislocation arrangement was recently confirmed by Jakobsen et al. [46] and Levine et al. [47]. The formation of a cell-wall structure is caused by the re-arrangement and re-grouping of dislocations. It changes the size of coherently-scattering regions, which is approximately equal to the average distance between the nearest dislocation walls. Intensity distribution of the peak depends on the kind of boundaries formed during the cell-wall structure formation. Diffraction by different kinds of dislocation walls was

Downloaded By: [Oak Ridge National Laboratory] At: 20:48 4 September 2009

Downloaded By: [Oak Ridge National Laboratory] At: 20:48 4 September 2009

described in the references [35–38]. If positions of dislocations within the cell-wall remain weakly correlated, they result in the intensity profiles similar to that of randomly distributed dislocations (although with some additional coefficients). Such walls are related to incidental dislocation boundaries (IDBs). To minimize the energy, dislocations within the wall typically re-arrange into strongly correlated thin walls. A correlation increase between the dislocation positions causes dramatic changes in the intensity profiles. In this case, the so-called equidistant-distribution of the same sign dislocations within the wall is formed with a higher misorientation through the boundary. Such equidistant-dislocation-wall relates to the thin cell-block boundary, and provides a finite sharp rotation between two parts of the crystal separated by the wall. The intensity profile of the peak caused by such equidistant-cell-block boundaries changes, and the central part of it follows the Lorentzian function

$$I(q_D) = I_{Di}\frac{q_{Di}}{\pi^2 q^2 + q_{Di}^2} \tag{3}$$

where q is the deviation of the diffraction vector from the exact Bragg position. Here the integral line width, q_{Di}, is given by [36,38]

$$q_{Di} = \pi\varsigma_{hkl}/D \tag{4}$$

where D is the average distance between walls. The contrast factor for the cell-wall structure, ς_{hkl}, depends on the kind of walls, elastic anisotropy of the matrix, and (hkl) of the reflection.

The Lorentzian type of intensity profiles can also be caused by the stacking faults. However, stacking faults should cause distinct anisotropic shifts of the different (hkl) peaks. For example, (222) and (200) peaks should shift in the opposite directions [33,35]. Hence, the effect of stacking faults can be separated from the effect caused by equidistant-dislocation-cell-boundaries; such opposite shift of (222) and (200) peaks was not observed in the experimental diffraction patterns. The values of the lattice parameter and strain were determined from different (hkl) reflections at different distances from the crack tip (Figure 2). The variation of lattice parameter and by inference residual strain is plotted in Figure 2 as a function of distance from the initial notch. We note that the data analysis typically determines an average lattice strain from the individual hkl measurements (Figure 2a–c). If however, we get the strain for the individual hkl reflections, there are small but significant variations (Figure 2d). These variations are consistent with the elastic compliances of the sample.

Experimental diffraction pattern was processed with a Rietveld method. Usually more than eight peaks were registered. All peaks were fitted to the pseudo-Voigt function, which allows separation of the Gaussian and the Lorentzian components. The Gaussian component was used to estimate the weakly correlated portion of the dislocation population located both in the cell interior and within the incidental dislocation boundaries of the so-called formal total dislocation density [34–37,41–45]. All possible dislocation slip systems with a typical Burgers vector for FCC structure $\mathbf{b}\|\langle 110\rangle$ were taken into account. Dislocation density values, determined for each hkl, separately, were slightly scattered within the error bars shown at the Figure 3(a). For better statistics these values were then averaged over different hkl for each location (Figure 3a). From the Lorentzian component, the size of coherently scattering domains and the distance between equidistant-dislocation-walls were found (Figure 3b).

Downloaded By: [Oak Ridge National Laboratory] At: 20:48 4 September 2009

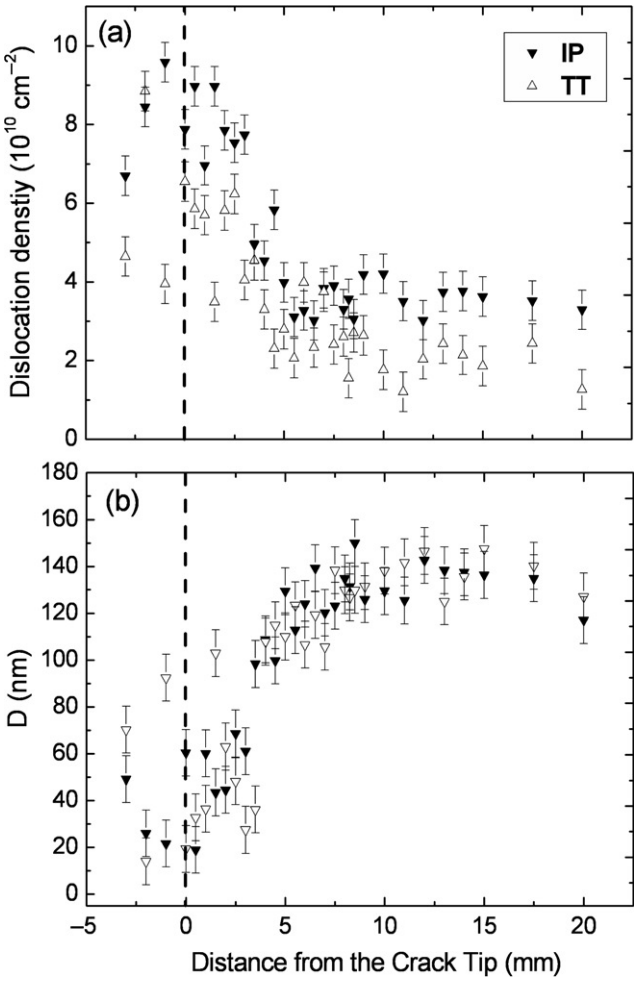

Figure 3. Dislocation density distribution for IP and TT directions as a function of distance from the crack tip immediately after overload (LP7 in Figure 1b) (a); distance between dislocation walls forming cell-wall structure (b).

The formal total dislocation density distribution profiles along IP and TT directions after the overload are shown in Figure 3(a). A higher value is observed near the crack tip. The maximal dislocation density reaches $10 \times 10^{10}\,\mathrm{cm}^{-2}$ at the crack tip. The high dislocation density is due to the large plastic deformation occurring at the crack tip during the overload. The overload-induced large plastic zone retards the crack propagation, because the crack has to grow out of such a plastic zone to resume a steady-state growth [48–53]. The estimated distance between the dislocation walls forming cell-wall structure is shown in Figure 3(b). The large plastic deformation and high-dislocation density near the crack tip enhance the self organization of the dislocations within dislocation walls and formation of the cell-wall structure. The intense formation of the equidistant-dislocation-walls forming geometrically necessary boundaries results in the decrease of the average distance between the dislocation walls in this region relative to its value in the remote areas

from the crack tip. Similar trend was observed during the fatigue test of HASTELLOY C-22HS alloy by Huang et al. [53]. This conclusion confirms an earlier observation of Groma and Szekely [42] for the deformed Cu single crystal that 'at a certain deformation level the dislocation density in the dense regions cannot increase any more...'. The TEM studies are on the way to complement the results of the dislocation arrangement analysis.

3.2. *Distribution of geometrically necessary dislocations and strain gradients from polychromatic X-ray microdiffraction*

To understand the behavior of the dislocation ensemble at the microscale, spatially-resolved 2D maps of strain gradients and GNDs distribution were recorded in 10 different areas neighboring the fractured surface after the crack propagation for both materials. At each area ~450 locations were probed with a step size of 1 μm in the directions parallel and perpendicular to the main crack propagation. The most interesting regions with a high density of GNDs were found in the areas neighboring the fractured surface along the crack propagation path. Numerous small voids and small cracks running approximately perpendicular to the main crack direction were observed. Strong lattice rotations of the order of several degrees were found within 20 μm from the fractured surface. To follow the depth dependence of GNDs distribution, 3D measurements with DAXM [23] were performed at different distances from the fractured surface (Figure 4). Dramatic changes occur within several microns of the fracture surface after crack propagation. The positions of the microprobe relative to the fractured surface are shown in Figure 4(a). The depth-integrated Laue patterns at distances of 5 and 10 μm from the fractured surface are distinct (Figure 4b and c). At the distance of 5 μm, significant 'streaking' is observed, which is an indication of strain gradients and a high density of GNDs in that region [21,22]. A sketch of the grain with a possible GNDs arrangement near the fractured surface providing lattice curvature near the fracture is presented in Figure 4(d). A similar shape of the near-fracture surface is observed experimentally. Depth-resolved images corresponding to every micrometer layer at different depths are shown in Figure 4(e). 3D measurements demonstrate that the layers with a high GND's density are located in the first 12 μm near the surface. At larger depth (17 μm) streaking disappears and orientation does not change significantly with further depth increase. Our observations for both ferritic steel and Ni-based superalloy show the same tendency for the depth dependence of the GND's distribution as the one observed by Mughrabi et al. [54] for deformed Cu.

3.3. *Cohesive interface model and finite element simulations*

The general deformation characteristics near a fatigue crack tip include a plastic zone in front of the crack tip and a plastic wake left behind, where the cyclic loading and fatigue crack growth lead to a compressive strain. The magnitude and distribution of the compressive strain in this plastic wake depend on the stress multiaxiality, material properties, and crack growth increment in each loading cycle. An irreversible and hysteretic cohesive-interface model is developed here to simulate the fatigue crack nucleation and growth, so that the deformation properties in the vicinity of the fatigue

Downloaded By: [Oak Ridge National Laboratory] At: 20:48 4 September 2009

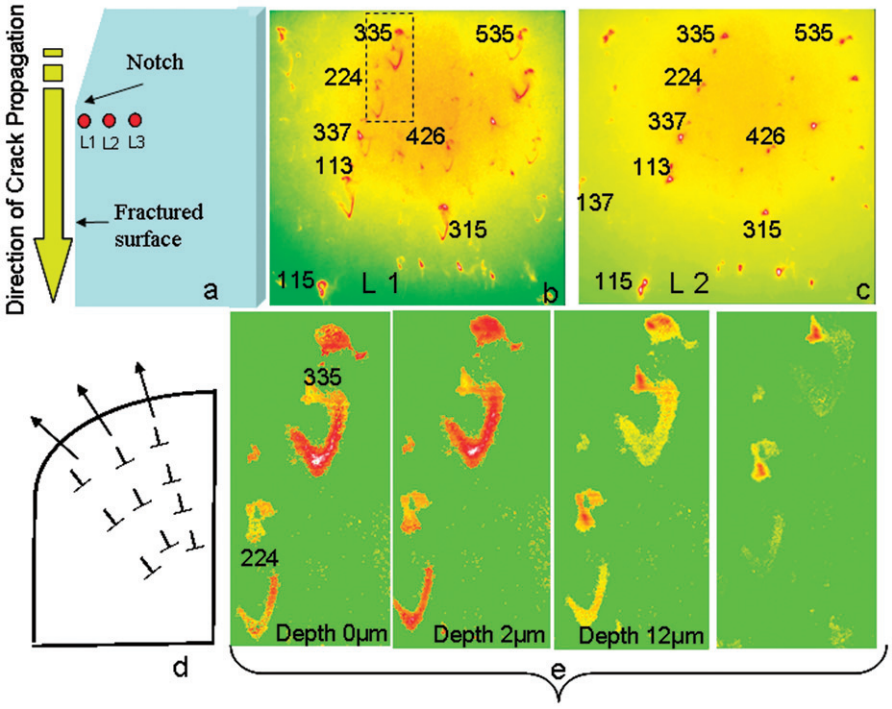

Figure 4. (a) Sketch of the fractured sample after crack propagation with probed locations at different distance from the fracture. Depth integrated Laue patterns obtained from locations at the distance: (b) 5 μm; (c) 10 μm from the fractured surface; (d) sketch of the grain near fracture surface with varying lattice curvature and GNDs density; (e) depth resolved images from the 1st location (L1) at different depths.

crack tip can be illustrated. In a general cohesive interface model, the crack is modeled by a set of cohesive interface elements, which separate according to the constitutive equations relating the tractions acting on the two bonded solids to the separation between them [23–26]. The nucleation and propagation of the crack are the natural result of the finite-element simulation, and no *ad hoc* fracture criterion is required. The cyclic loading will have no effect on the crack behavior if the cohesive constitutive law is reversible. However, an irreversible cohesive model will eventually lead to plastic shakedown; the crack arrests after a finite number of cycles. Following the work in [23,24], the introduction of an irreversible cohesive law with unloading–reloading hysteresis gives a phenomenological means to accumulate crack tip damage and thus to allow a steady crack growth and the development of a plastic wake when the applied stress-intensity-factor is in a range that is smaller than the intrinsic fracture toughness.

During monotonic loading, the traction T_n and separation Δ_n are related by $T_n = \sigma_{\max}\frac{\Delta_n}{\delta_n}\exp(1-\frac{\Delta_n}{\delta_n})$, where $\sigma_{\max}$ is the interface strength and δ_n is a characteristic length scale. During unloading and reloading, we specify

$$\dot{T}_n = \begin{cases} K^-\dot{\Delta}_n, & \dot{\Delta}_n < 0 \\ K^+\dot{\Delta}_n, & \dot{\Delta}_n > 0 \end{cases} \tag{5}$$

Downloaded By: [Oak Ridge National Laboratory] At: 20:48 4 September 2009

where the unloading stiffness is determined by the unloading point, $K^- = T_n^{\text{unload}}/\Delta_n^{\text{unload}}$, while the reloading stiffness is given by the following evolution equation:

$$\dot{K}^+ = \begin{cases} -K^+ \frac{\dot{\Delta}_n}{\delta_f}, & \dot{\Delta}_n > 0 \\ (K^+ - K^-)\frac{\dot{\Delta}_n}{\delta_a}, & \dot{\Delta}_n < 0 \end{cases}, \tag{6}$$

where δ_f and δ_a are two length parameters that characterize the damage behavior. The above irreversible, hysteretic cohesive model has been implemented into the commercial FEM software, ABAQUS, through a user-define element (UEL) subroutine. The divergence problem associated with crack nucleation in the finite element simulation is regularized by adding a fictitious viscous term in the traction-separation law [25,26].

For a fatigue crack to grow steadily, we need to ensure that the plastic wake size is at least twice that of the plastic zone size, the cracking bridging size is much smaller than the plastic zone size, and the crack increment in a cycle (and also that in the overload cycle) is much smaller than the plastic zone size. As long as these three conditions are met, the strain distributions near the stable fatigue crack growth will be insensitive to the cohesive parameters. To this end, we chose $\sigma_{\max} = 840$ MPa, $\delta_n = 1$ μm, $\delta_a/\delta_n = 0.1$ (so that during unloading, K^+ quickly approaches K^-), and $\delta_f/\delta_n = 25$ (K^+ slowly degrades during loading), and thus a steady plastic wake can be developed within a meaningful computation time. The surrounding material is modeled by the elastic-perfectly plastic behavior, with the elastic modulus $E = 210$ GPa, Poisson's ratio $\nu = 0.33$, and yield stress $\sigma_Y = 288$ MPa. Consequently, the plastic dissipation adjacent to the fatigue crack tip is computed explicitly and independently from the cohesive separation processes.

After the crack propagates to a length similar to that Figure 1, an overload of 1.33 $P_{\max}$ was imposed. Figure 5(a) shows the elastic strain distribution $\varepsilon_{22}^{\text{elastic}}$ (where subscript 2 denotes the IP direction) at the minimum loads before and after the overload. The simulation results are intended to compare to the neutron experiments in Figures 1 and 2, where the strains are a result of an average over a gauge volume of $1 \times 1 \times 2$ mm. For this reason, strains in Figure 5(a) are generated by averaging the strains

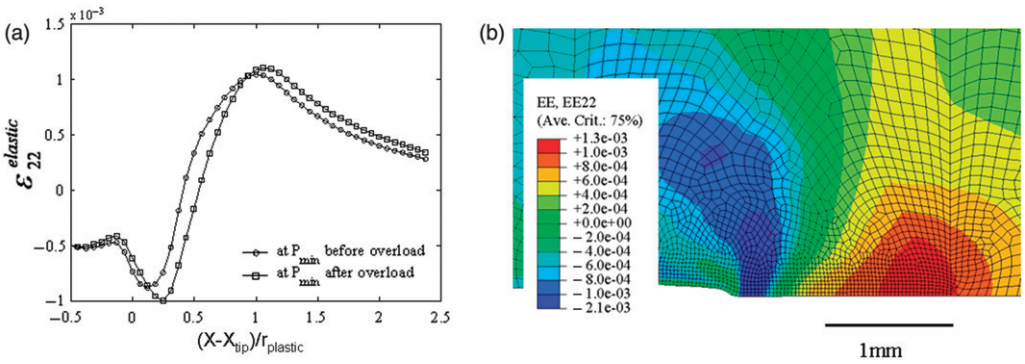

Figure 5. (a) The distributions of elastic strain, $\varepsilon_{22}^{\text{elastic}}$, at the minimum loads immediately before and after the overload, as calculated by the cohesive interface model in Equations (5) and (6). The compressive strain is observed ahead of the fatigue crack tip, and the overload causes an increase of the elastic strain field. (b) The contour plot of $\varepsilon_{22}^{\text{elastic}}$ at the minimum load before the overload on the deformed mesh where the displacement is magnified by a factor of 10.

Downloaded By: [Oak Ridge National Laboratory] At: 20:48 4 September 2009

in a 1×1 mm area. The abscissa is normalized by the plastic zone size at the maximum load in the cycle prior to the application of the overload, i.e., $r_{\text{plastic}} \approx 1.8$ mm. The crack tip location is determined when the crack opening displacement is equal to $2\delta_n$. A 2D contour plot of the elastic strain field at the minium load prior to the overload is given in Figure 5(b), where the crack opening profile can be easily seen. Comparisons between Figures 2 and 5 show the same trends in the development of the compressive residual strain in the plastic wake behind the crack tip and the tensile strain at about r_{plastic} ahead of the crack tip. If the plastic wake is not developed, the compressive strain will not be observed. The slight difference between the magnitude of predicted and measured strains is due to the use of plane strain condition in the simulation, while the experimental setup leads to a mixture of plane stress condition near the free surface and plane strain condition inside the plate. Exactly for the same reason, the calculated plastic zone size is smaller than the measured value.

The application of the overload produces a large plastic zone. During unloading, this plastic zone tends to maintain its permanent deformation, while the surrounding elastic deformation zone tends to shrink. Consequently, a large compressive strain will be superposed onto this zone, which is observed both experimentally and in the finite element simulations. However, our simulations show a small shift in the peak of the elastic strain, while experimentally a large shift is observed. This can be understood by the boundary condition. In the experimental setup, the applied overload leads to a large plastic zone which extends to half of the way to the free boundary. Consequently, a large tensile strain is resulted to balance the compressive strain near the free boundary. To quantitatively compare neutron strain measurements and finite element simulations, a 3D boundary value problem needs to be solved, which is left for a future study.

4. Summary

In summary, the physical mechanisms of the plasticity-induced crack-'closure' resulting in the retardation of the crack propagation were investigated using the neutron and X-ray microbeam diffraction techniques and finite element simulations. The connection among these three techniques lies at the development of the residual stress distribution around a fatigue crack tip with and/or without an overload. Both neutron experiments and finite element simulations agree on the strain distribution in the plastic wake and the overload-induced compressive residual strain. The fatigue overload produces a large plastic zone, which has been observed from plastic strains and the dislocation density distributions. The overload-induced plastic deformation results in compressive elastic strains in front of the crack tip. Our cohesive interface model and the resulting finite element simulations qualitatively capture the trends in the distribution of elastic and plastic strains in the vicinity of the crack tip during fatigue and overload. The compressive elastic strains and large plastic zones are responsible for the retardation of the post-overload crack propagation. Strain gradients in the region of the crack propagation result in the formation of high density of GNDs, microcracks, and lattice rotations reaching several degrees within 20 μm zone near the fracture. Depth resolved measurements reveal strain gradients and a high density of GNDs in the first 12 micrometers under the surface.

Downloaded By: [Oak Ridge National Laboratory] At: 20:48 4 September 2009

Acknowledgements

The authors would like to acknowledge the financial supports from the NSF International Materials Institutes (IMI) Program (DMR 0231320). Research at Oak Ridge National Laboratory is sponsored by the Division of Materials Sciences and Engineering, Office of Basic Energy Sciences, U.S. Department of Energy, under Contract DE-AC05-00OR22725 with UT-Battelle, LLC.

References

[1] S. Suresh, *Fatigue of Materials*, 2nd ed., Cambridge University Press, New York, USA, 1998.
[2] J. Schijve, D. Broek and P. Rijk de, Report No NLR-TN M, National Aero- and Astronautical Research Institute, Amsterdam, 1961, p.2094.
[3] R.C. Rice and R.I. Stevens, ASTM STP 536 (1973) p.95.
[4] S. Suresh, G.F. Zamiski and R.O. Ritchie, Metall. Mater. Sci. 12 (1981) p.1435.
[5] W.A. Logsdon and P.K. Liaw, Eng. Fract. Mech. 24 (1986) p.737.
[6] P.K. Liaw, T.R. Leax, R.S. Williams et al., Metall. Trans. A – Phys. Metall. Mater. Sci. 13 (1982) p.1607.
[7] P.K. Liaw, T.R. Leax and W.A. Logsdon, Acta Metall. 31 (1983) p.1581.
[8] W.A. Logsdon, P.K. Liaw and M.A. Burke, Eng. Fract. Mech. 36 (1990) p.183.
[9] P.K. Liaw, S.J. Hudak and J.K. Donald, Metall. Trans. A – Phys. Metall. Mater. Sci. 13 (1982) p.1633.
[10] P.K. Liaw, A. Saxena, V.P. Swaminathan et al., Metall. Trans. A – Phys. Metall. Mater. Sci. 14 (1983) p.1631.
[11] P.K. Liaw, T.R. Leax, R.S. Williams et al., Acta Metall. 30 (1982) p.2071.
[12] W. Woo, H. Choo, D.W. Brown et al., Appl. Phys. Lett. 86 (2005) p.231902.
[13] H. Choo, D. Seo, J. Beddoes et al., Appl. Phys. Lett. 85 (2004) p.4654.
[14] D.J. Smith, R.H. Leggatt, G.A. Webster et al., J. Strain Anal. Eng. Design 23 (1988) p.201.
[15] M. Ceretti, C.A. Hippsley, M.T. Hutchings et al., Physica B 234–236 (1997) p.969.
[16] D.J. Smith, M.A.M. Bourke, A.P. Hodgson et al., J. Strain Anal. 27 (1992) p.77.
[17] H. Choo, M. Bourke, P. Nash et al., Mater. Sci. Eng. A – Struct. Mater. Properties Microstruct. Process. 264 (1999) p.108.
[18] J. Smith, M.N. Bassim, C.D. Liu et al., Eng. Fract. Mech. 52 (1995) p.843.
[19] P.W. Stephens, J. Appl. Cryst. 32 (1999) p.281.
[20] G.E. Ice and R.I. Barabash, *White beam microdiffraction and dislocations gradients*, in *Dislocations in Solids*, F.R.N. Nabarro and J.P. Hirth, eds., Vol. 13, Chapter 79, Elsevier, Amsterdam, New York, 2007, p.500.
[21] R.I. Barabash, G.E. Ice and J.W.L. Pang, Mater. Sci. Eng. A-Struct. Mater. Properties Microstruct. Process. 400 (2005) p.125.
[22] W. Yang, B.C. Larson, J.Z. Tischler et al., Micron 35 (2004) p.431.
[23] O. Nguyen, E.A. Repetto, M. Ortiz et al., Int. J. Fract. 110 (2001) p.351.
[24] S. Serebrinsky and M. Ortiz, Scripta Mater. 53 (2005) p.1193.
[25] Y.F. Gao and A.F. Bower, Model. Simul. Mater. Sci. Eng. 12 (2004) p.453.
[26] S.M. Xia, Y.F. Gao, A.F. Bower et al., Int. J. Solids Struct. 44 (2007) p.3685.
[27] M.A.M. Bourke, D.C. Dunand and E. Ustundag, Appl. Phys. Letters 74A (2002) p.S1707.
[28] H.M. Rietveld, J. Appl. Cryst. 2 (1969) p.65.
[29] M.T. Hutchings, P.J. Withers, T.M. Holden et al., *Introduction to the Characterization of Residual Stress by Neutron Diffraction*, Taylor & Francis Group, CRC Press, Boca Raton, FL, USA, 2005.
[30] P. Klimanek, T. Kschidock, P. Mikula et al., Physica B 234–236 (1997) p.965.
[31] D. Breuer and P. Klimanek, Mat. Sci. Eng. A234–236 (1997) p.818.

Downloaded By: [Oak Ridge National Laboratory] At: 20:48 4 September 2009

[32] P. Klimanek, T. Kschidock, P. Lukas et al., J. Phys. IV, Colloque C7, Supplement of J. Phys. III 3 (1993) p.2143.
[33] B.E. Warren, *X-ray Diffraction*, Dover Publications, Inc., New York, 1969, p.381.
[34] M. Wilkens, Phys. Stat. Sol. A 2 (1970) p.359.
[35] M.A. Krivoglaz, *Theory of Scattering of X-rays and Thermal Neutron Scattering by Real Crystal*, Plenum Press, New York (1969), 1996.
[36] M.A. Krivoglaz, K.P. Ryaboshapka and R.I. Barabash, Phys. Met. Mettallogr. 30 (1970) p.1134.
[37] R.I. Barabash and M.A. Krivoglaz, Metallofizika 4 (1983) p.3.
[38] R.I. Barabash and P. Klimanek, J. Appl. Cryst. 32 (1999) p.1050.
[39] P. Klimanek and R. Kuzel Jr, J. Appl. Cryst. 21 (1989) p.47.
[40] P. Klimanek, R.I. Barabash, D. Breuer et al., Proceedings of the 20th Riso International Symposium of Materials and Sciences, Riso National Laboratory, Roskilde DK, 1999 p.381.
[41] M. Wilkens, T. Ungar and H. Mughrabi, Phys. Status Sol. A 104 (1987) p.157.
[42] I. Groma and F. Szekely, J. Appl. Cryst. 33b (2000) p.1329; Scripta Mater. 54 (2006) p.753.
[43] T. Ungar, I. Groma and M. Wilkens, J. Appl. Cryst. 22 (1989) p.26.
[44] H. Mughrabi, Acta Metall. 31 (1983) p.1367.
[45] H. Mughrabi, T. Ungar, W. Kienle et al., Phil. Mag. A. 53 (1986) p.793.
[46] B. Jakobsen, U. Lienert, J. Almer et al., Science 312 (2006) p.889.
[47] L. Levine, B.C. Larson, W. Yang et al., Nat. Mater. 5 (2006) p.619.
[48] Y. Sun, H. Choo, P.K. Liaw et al., Scripta Mater. 53 (2005) p.971.
[49] Y. Sun, R. Barabash, H. Choo et al., Solid State Phenom. 129 (2007) p.151.
[50] T. Anderson, *Fracture Mechanics: Fundamentals and Application*, Boca CRC Press, Boca Raton, 1995.
[51] J. Willenborg, R.M. Engle and H. Wood, Technical Report TFR, North American Rockwell, LosAngeles, 1971 p.701.
[52] E. Wheeler, J. Basic Eng. 94 (1972) p.181.
[53] E.-W. Huang, R.I. Barabash, Y. Wang et al., Int. J. Plasticity 24 (2008) p.1440.
[54] H. Mughrabi, T. Ungar and M. Wilkens, Scripta Metall. 17 (1983) p.797.

Downloaded By: [Oak Ridge National Laboratory] At: 20:48 4 September 2009